Inorganic Chemistry

Article

pubs.acs.org/IC

Electronic Structure and Magnetic Properties of $CuFeS_2$

Sergio Conejeros,[†] Pere Alemany,*[,†] Miquel Llunell,[†] Ibério de P. R. Moreira,*[,†] Víctor Sánchez,[‡] and Jaime Llanos[‡]

[†]Departament de Química Física and Institut de Química Teòrica i Computacional (IQTCUB), Universitat de Barcelona, Diagonal 647, 08028 Barcelona, Spain

[‡]Departamento de Química, Facultad de Ciencias, Universidad Católica del Norte, Casilla 1280, Antofagasta, Chile

Supporting Information

ABSTRACT: Chalcopyrite ($CuFeS_2$) is an antiferromagnetic semiconductor with unusual magnetic and electrical properties, which are still not clearly understood. Neutron diffraction experiments reveal a phase transition at ~50 K that has been attributed to an unexpected appearance of magnetic moments on Cu ions, having a paramagnetic arrangement down to 50 K and then ordering to an antiferromagnetic state at lower temperatures. In this study we use DFT-based computational methods to investigate the electronic structure and magnetic properties of $CuFeS_2$ in order to obtain a reliable source of information for the interpretation of the observed magnetic behavior, and in particular to shed some light on the magnetic behavior of copper atoms in this compound. We have calculated the electronic structure of the ground and low-energy magnetically excited states and deduced a set of exchange coupling constants that are used afterward in classical Monte Carlo simulations to obtain magnetic susceptibility data, which compare successfully with our experimental results above ~170 K. From our results it can be inferred that copper atoms remain in a diamagnetic state in this temperature range, although spin delocalization from neighboring iron atoms results in a non-negligible spin density on the copper atoms at high temperatures.

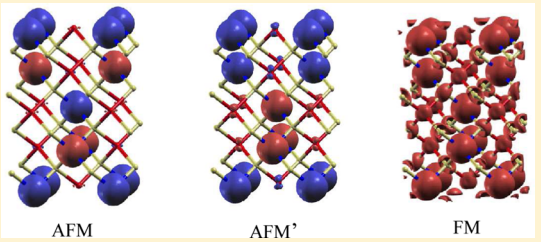

1. INTRODUCTION

Transition-metal sulfides are an important class of Earth materials with a fascinating diversity of structure types[1] that exhibit a host of technologically relevant electronic, magnetic, and catalytic properties. Because of the prominent role of sulfides as a source of nonferrous metals, the oxidation state of metals in these compounds has been extensively used in order to rationalize their fundamental crystal properties, the processes of mineral formation and breakdown, mineral processing, and their participation in environmental contamination associated with mining activities. However, it is surprising to find that, after numerous studies, there is still some debate on the assignation of oxidation states in a common mineral of prominent economic relevance such as chalcopyrite ($CuFeS_2$), which represents the bulk of the world supplies of copper.[2]

Chalcopyrite is an antiferromagnetic semiconductor that crystallizes in a zincblende-type structure with four-coordinate cations and anions forming distinct corner-sharing tetrahedra[3] whose unusual magnetic and electrical properties are still not yet completely understood. $CuFeS_2$ exhibits a complex antiferromagnetic behavior, and neutron diffraction experiments reveal an effective magnetic moment for Fe of 3.85 μ_B,[4] which is unusually low in comparison to the expected value for Fe^{3+} ions (~5.0 μ_B). However, Mössbauer spectroscopy studies show without any doubt that iron in chalcopyrite is trivalent and is in a high-spin state.[5,6] In fact, some authors[6−8] attribute the observed low Fe moment to a substantial covalent character of Fe−S interactions. On the other hand, the valence state of the Cu ion is still a matter of controversy. From neutron powder diffraction results, some authors have reported a small moment on the copper ion.[4,9,10] Woolley et al.[9] proposed a paramagnetic arrangement down to 50 K and then ordering to an antiferromagnetic form at lower temperatures. However, Knight et al.[10] suggested that the magnitude of the magnetic moment on Cu remains debatable, since powder neutron diffraction is too insensitive to clarify the possibly small moment carried by the copper ion in the presence of the large moment of the iron ion.

Supporting the proposal given by Woolley, a cusp-like anomaly observed at ~50 K in the magnetic susceptibility of chalcopyrite has been interpreted as the onset of additional antiferromagnetic ordering attributed to the copper ions. Therefore, the presence of Cu^{2+} ions is suggested, since Cu^{+} ions have diamagnetic behavior.

Recently, Lovesey et al.[11] with their X-ray absorption spectra results have shown that between 10 and 65 K the copper ions remain monovalent ($3d^{10}$) and, consequently, a valence transition and the subsequent ordering of the copper moments as the origin of the low-temperature phase ($T_c \approx 50$ K) can be ruled out. However, the cusplike anomaly observed in the magnetic susceptibility at ~50 K remains unclear.

Received: February 18, 2015
Published: May 5, 2015

DOI: 10.1021/acs.inorgchem.5b00399
Inorg. Chem. 2015, 54, 4840−4849

In order to shed some light on all of these questions, in this work we provide a thorough computational study of the electronic structure of $CuFeS_2$ that, in our opinion, provides an insight into the physical mechanisms responsible for the unusual magnetic properties of $CuFeS_2$ by linking spin density topologies to the macroscopic magnetic behavior of the system. We further apply a methodological scheme based on density functional theory (DFT) combined with classical Monte Carlo simulations (CMC) to calculate magnetic susceptibility (χ) curves for $CuFeS_2$. Magnetic exchange coupling constants are calculated through state-of-the-art first-principles DFT-based methods and then inserted in the CMC scheme to simulate the behavior of χ with temperature in $CuFeS_2$. We also present new experimental magnetic susceptibility data for pure $CuFeS_2$ samples in order to compare with our theoretical results and to rule out the possibility of artifacts in the interpretation of earlier magnetic susceptibility measurements for natural samples of chalcopyrite due to the presence of magnetic impurities.[10,12−14]

2. CRYSTAL STRUCTURES AND PROPERTIES

$CuFeS_2$ crystallizes in the tetragonal space group $I\bar{4}2d$ (122), and its crystal structure (Figure 1) can be derived from that of zincblende by doubling the unit cell in the direction of the c axis. In this structure, copper and iron ions occupy the centers of MS_4 tetrahedra that share vertices. The magnetic structure of chalcopyrite has been determined by neutron diffraction by several authors,[4,8−10] whose results indicate that the spins on any two iron atoms bonded to a common sulfur atom are opposed and directed along the c axis (Figure 1). The shortest Fe−Fe distance is 3.71 Å, too long for direct exchange through overlap of atomic orbitals, and coupling between nearest neighbors is attributed to the superexchange type via the 110.7° Fe−S−Fe pathway, which for high-spin d^5 ions is predicted to be antiferromagnetic.[8] As mentioned in the Introduction, some studies suggest the existence of a small magnetic moment on the copper atoms with values between 0.05 and 0.2 μ_B,[4,9,14] although there is no consensus on this issue. For simplicity, in Figure 1 we only consider Cu^+, Fe^{3+}, and S^{2-} ions and show the antiferromagnetic ordering of the Fe^{3+} magnetic moments.

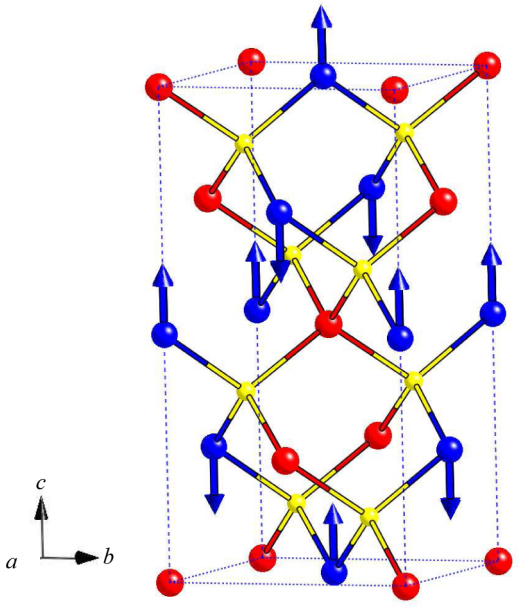

Figure 1. Unit cell of $CuFeS_2$ showing the antiferromagnetic ordering of Fe^{3+} ions only. Blue balls correspond to iron ions, and the arrows indicate the direction of the $S = 5/2$ spins in the antiferromagnetic ground state. Red balls correspond to copper ions and small yellow balls to sulfide ions.

Nikiforov[15] has critically reviewed the experimental studies of the electrical, optical, and magnetic properties as well as electronic structure calculations prior to 1999. In further experimental studies, the oxidation states of the metals in $CuFeS_2$ and related materials have been extensively discussed on the basis of different X-ray spectroscopy experiments: e.g., X-ray photoelectron spectroscopy (XPS),[2,6,16,17] X-ray absorption spectroscopy (XAS),[2,11] X-ray absorption near-edge structure (XANES),[18,19] and near-edge X-ray absorption fine structure (NEXAFS).[19,20] The oxidation states of copper and iron in $CuFeS_2$ deduced from these experimental techniques are nevertheless still a matter of controversy. Most of the spectroscopic results coming from XPS and XAS studies indicate that the oxidation state of copper in chalcopyrite is Cu^+. In addition, Mössbauer spectroscopy studies at room temperature resulted in a six-line spectrum, which indicates that iron ions in $CuFeS_2$ are undoubtedly in a trivalent, magnetically ordered state.[6] However, some other authors have argued cogently a $Cu^{2+}Fe^{2+}S_2$ composition on the basis of X-ray absorption spectroscopic (XAS) evidence.[18,19]

Sato et al.[7] carried out resonant X-ray emission spectroscopy (RXES) experiments and analyzed them by means of cluster-model calculations with configuration interaction (CI) wave functions to explain the overlapping d−d and charge transfer transitions, which cannot be observed by conventional optical absorption experiments. According to their calculations, they found for the ground state a predominant (54.6%) character for the Fe $3d^6\underline{L}$ ($\underline{L}$ = ligand hole) configuration. The significant S (3p) to Fe (3d) charge transfer is suggested in this study to be a dominant cause of the unusual 3d electron behavior in this material. This hybridization would result in lower and higher electron densities on the S and Fe atoms, respectively, in comparison to those expected for a strongly ionic compound, explaining the reduced magnetic moment found for Fe atoms in chalcopyrite. In addition, taking into consideration the model proposed by Haldane and Anderson,[21] they arrived at the conclusion that $CuFeS_2$ is a Haldane−Anderson insulator with a negative charge transfer energy ($\Delta = -3$ eV). These results obtained for a cluster model provide meaningful clues to the nature of the Fe−S bonding in chalcopyrite. However, a more complete description of the material is required to provide a general picture of the electronic structure of the material and, in particular, on the oxidation state of copper ions.

3. EXPERIMENTAL SECTION

3.1. Experimental Procedure and Characterization. Since attempts to obtain good-quality crystalline samples of synthetic chalcopyrite yielded in all cases samples with a low crystallinity, polycrystalline samples of natural chalcopyrite from a deposit located in northern Chile have been used for the measurement of the magnetic susceptibility. Powder X-ray diffraction patterns were collected with a Bruker AXS D8 Advance diffractometer in the 2θ range from 10 to 90°, with Cu Kα radiation (λ = 0.15045 nm), operating at 40 kV and 30 mA. All measurements were carried out at room temperature. According to the X-ray analysis (see Figure S1 in the Supporting Information) these samples show a high purity with no evidence of relevant chemical impurities. Before performing the magnetization measurements, we divided the sample in two parts of 252 mg (sample

DOI: 10.1021/acs.inorgchem.5b00399
Inorg. Chem. 2015, 54, 4840−4849

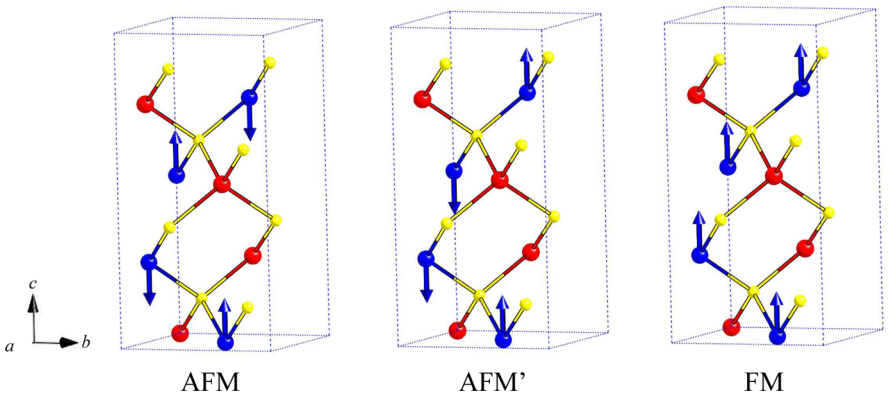

Figure 2. Schematic representations of the three spin configurations considered in the calculations using the conventional cell.

1) and 93.2 mg (sample 2), respectively. Then, the magnetic susceptibility was measured using a SQUID magnetometer. Temperature-dependent data were collected after zero field cooling (ZFC) and field cooling (FC) between 5 and 300 K, with applied fields of 100 and 5000 Oe. The molar magnetic susceptibility was corrected for diamagnetism of the constituting atoms (Cu^{+}, -12×10^{-6} emu/mol; Fe^{3+}, -10×10^{-6} emu/mol; S^{2-}, -30×10^{-6} emu/mol).[22]

3.2. Computational Details. Calculations involving a single conventional crystallographic unit cell have been performed using the CRYSTAL09 code[23−25] to evaluate the electronic and magnetic properties of $CuFeS_2$. Relative energies of the different spin arrangements for the unpaired electrons were obtained applying density functional theory (DFT), adopting the hybrid B3LYP functional,[26] and all-electron atomic Gaussian basis sets. The basis sets used were of 8-6-411-(41d)G, 8-6-4111-(41d)G, and 8-6-311-G* quality optimized for Fe^{3+}, Cu^{+}, and S^{2-}, respectively.[23] For the calculation of the Coulomb and exchange integrals, ITOL1-5 tolerance factors of 7, 7, 7, 7, and 14 were used. The convergence criterion for the energy was set at 10^{-7} au.[25] Integration of k-dependent magnitudes has been carried out using a mesh of 260 k points in the irreducible Brillouin zone chosen according to the Monkhorst−Pack scheme[27] for all magnetic solutions.

Since it is not possible to obtain a set of independent equations to compute a complete set of all relevant magnetic exchange coupling constants between the iron atoms using a single unit cell, for this purpose we considered a $2 \times 1 \times 1$ supercell. In order to reduce the computational cost, these supercell calculations were performed using SIESTA,[28−30] a program that uses a numerical atomic orbitals DFT-based approach that has been developed for efficient calculations in large systems. The generalized gradient approximation to DFT and, in particular, the functional of Perdew, Burke, and Ernzerhof (PBE) has been used in all calculations.[31] In order to obtain a set of energies for the magnetic states similar to that calculated using the hybrid B3LYP functional, a Hubbard correction term,[32,33] $U_{eff} = U - J = 4.3$ eV, has been considered for the Fe (3d) states[34] in the supercell calculations. Calculations including a Hubbard term for Cu atoms with U_{eff} up to 8 eV did not result in any significant difference either in the atomic populations or in the relative energies of the considered states, and for this reason they will not be further discussed in the following. The contribution of core electrons in these calculations has been described by norm-conserving Troullier−Martins pseudopotentials[35] factorized in the Kleinman−Bylander form.[36] Valence electrons were treated explicitly using a split-valence basis set of triple-ξ plus polarization functions for copper and iron atoms and of double-ξ plus polarization functions for sulfur atoms, all of them obtained with an energy shift of 50 meV.[37] The energy cutoff for the real space integration mesh was set to 150 Ry, and the Brillouin zone was sampled with a mesh of 256 k points obtained using the method of Monkhorst and Pack.[27]

In both computational schemes, the spin-polarized formalism was used to describe symmetry-broken magnetic solutions with different localized spin orderings, whereas the diamagnetic state corresponds to the closed-shell solution obtained from the restricted formalism.

In order to obtain the magnetic susceptibility curve from the calculated magnetic exchange coupling constants, we have performed Monte Carlo simulations using a classical Heisenberg model as implemented in the ALPS code.[38] The simulations were made using a $8 \times 8 \times 8$ network of paramagnetic centers, including periodic boundary conditions and considering only the Fe centers with $S = 5/2$. The use of classical Monte Carlo simulations to obtain the magnetic susceptibility curve is justified for systems with large local spins, as in our case,[39,40] except perhaps at low temperatures, where quantum effects are dominant.

4. RESULTS AND DISCUSSION

4.1. Electronic and Magnetic Properties. The first step in order to gain some insight into the electronic structure and magnetic properties of chalcopyrite has been the evaluation of the relative stability of the most relevant magnetic solutions expected for this system.

For this purpose, the spin configurations corresponding to the ferromagnetic (FM), antiferromagnetic (AFM and AFM′), and nonmagnetic (diamagnetic) phases (Figure 2) were initially assigned to the four Fe atoms in the conventional unit cell. We have also tried to obtain solutions of the Kohn−Sham equations corresponding to ferrimagnetic states by forcing different combinations of high- and low-spin states on Fe ions, but it has not been possible to reach self-consistent convergence for any of these cases and they will not be further considered. We have also explored the possibility of ferrimagnetic states with local Fe(II) and Cu(II) configurations, but in all cases the SCF procedure converged to one of the three Fe(III)/Cu(I) solutions shown in Figure 2. Using a $2 \times 1 \times 1$ supercell that contains eight Fe atoms, it is possible to obtain additional spin configurations (see Figure 5), but due to the large computational requirements of the B3LYP hybrid functional, we only carried out these calculations using the PBE +U method using the SIESTA program.

By comparison of the total energies for the different magnetic states that can be obtained for a single unit cell (Table 1), it is evident that the closed-shell, diamagnetic solution lies considerably higher in energy than those where spin-polarization is allowed. The lowest energy (ground state) corresponds to the antiferromagnetic configuration labeled as AFM in Figure 2. In this state, the direction of the spins on the iron ions alternates between each layer perpendicular to the crystallographic c direction. This predicted ground state is in good agreement with experiments[4,8,9] where $CuFeS_2$ is found to be antiferromagnetic with the magnetic moments of the Fe centers directed along the c axis.

DOI: 10.1021/acs.inorgchem.5b00399
Inorg. Chem. 2015, 54, 4840−4849

Table 1. Relative Energies per Formula Unit for the Magnetic Configurations of $CuFeS_2$ Calculated for the Crystallographic Unit Cell using CRYSTAL with the B3LYP Functional and for the 2 × 1 × 1 Supercell using SIESTA with the PBE+U Functional

	E (meV)	
	B3LYP	PBE+U
diamagnetic	2539	2716
FM	445	400
AFM′	183	151
AFM	0	0

In order to check if calculations using SIESTA with the PBE+U functional are comparable to those obtained with CRYSTAL using the hybrid B3LYP functional, we also include in Table 1 the relative energies of the same four states calculated with this alternative approach. As seen in the table, the energy ordering of the four states and the energy differences between them are comparable using either method.

As shown in Table 2, chalcopyrite is predicted to be a semiconductor in the AFM ground state, in good agreement with the experimental findings, although the gap ($\Delta_{exp} \approx 0.5$ eV)[41] is somewhat overestimated, using both the B3LYP and the PBE+U methods. At this point it is important to remark that pure DFT methods underestimate the band gap in $CuFeS_2$,[42−45] providing a poor description of its electronic properties. In fact, in previous studies $CuFeS_2$ has even been predicted to be a metal, in contrast to the experimental findings.[42,45] Furthermore, we find that the band gap values of $CuFeS_2$ are strongly dependent on the spin arrangement of the iron ions, decreasing from the AFM to the FM phase. This trend, on one hand, is due to the energy of the α valence band that increases in the AFM′ (0.05 eV) and FM (0.68 eV) configurations relative to the AFM configuration (0.00 eV) and, on the other hand, to the fact that the bands of the conduction band in the AFM′ and FM configurations have slightly stronger dispersions in comparison to that in the AFM case. The calculated bandwidth values are 1.2, 1.9, and 3.2 eV for AFM, AFM′, and FM, respectively, and the bottom of the conduction band is pushed down by 0.39 and 0.90 eV for the AFM′ and FM configurations, respectively. For all three states, the individual orbital contributions near the Fermi level are similar, with the top of the valence band dominated by Cu(3d) and S(3p) levels (Figure 3) and the bottom of the conduction band arising mainly from the Fe(3d) levels.

Table 2. Calculated Values of Band Gap (Δ) and Final Spin Densities (ρ) for Fe−Cu−S Atoms Obtained from a Mulliken Population Analysis for the Antiferromagnetic and Ferromagnetic Configurations of $CuFeS_2$

	B3LYP		PBE+U	
	Δ (eV)	ρ	Δ (eV)	ρ
FM	0.20	3.89−0.26−0.42	metallic	4.12−0.27−0.31
AFM′	1.32	3.80−0.10−0.33	0.61	3.99−0.07−0.20
AFM	1.82	3.75−0.00−0.00	0.94	3.93−0.00−0.00

Previously published works,[42−45] exploring the electronic structure of $CuFeS_2$ for the AFM ground state using pure DFT methods, have reported values for spin densities obtained from population analysis between 3.1 and 3.3 unpaired electrons for the Fe sites, which are significantly lower than the values of around 3.8 obtained in our calculations, using either the B3LYP or the PBE+U method, which are, however, in good agreement with the effective magnetic moment for Fe of 3.85 μ_B determined from experimental data.[4] The differences between previous computational studies and our values arise from the well-known trend of pure DFT functionals to lead to an exceedingly large delocalization of the electron density, a feature that is in part corrected by either introducing an on-site Hubbard term on the 3d levels of iron or using an hybrid exchange-correlation potential such as B3LYP.[46]

For the AFM ground state, the spin densities for the Fe, Cu, and S atoms presented in Table 2 indicate, as expected, a diamagnetic d^{10} electronic configuration for copper, i.e. a Cu^+ oxidation state, while the population on Fe ions is compatible with a d^5 electronic configuration corresponding to Fe^{3+}. The calculated spin densities are, as noted above, lower than those expected for free Fe^{3+} ions (5.0 μ_B). This can be interpreted as a direct consequence of the non-negligible degree of covalency of the Fe−S bonds in chalcopyrite. The significant effect of the covalency of M−S interactions on the magnetic moment of the Fe^{3+} ions can be easily visualized by comparing our results for Fe^{3+} coordinated by sulfur atoms with those obtained for a case in which Fe^{3+} is coordinated to the more electronegative oxygen atom. Catti et al. report a value of 4.74 unpaired electrons per Fe^{3+} ion for α-Fe_2O_3 (hematite) using the UHF method and Mulliken population analysis for the AFM ground state.[47] We have used the same crystal structure and basis sets as in ref 47 to perform PBE0 calculations, and the Mulliken population analysis on the AFM lowest energy magnetic solution gives 4.29 unpaired electrons to each Fe^{3+} ion, a value that is somewhat lower, 4.20, when using the B3LYP functional. The experimental value for the magnetic moment of Fe^{3+} is 4.9 μ_B, very close to that expected for the free ion.

From this analysis, it is easy to conclude that a consistent ionic formula for the AFM phase is $Cu^+Fe^{3+}(S^{2-})_2$, although in this case this is just a formal description of the electronic structure that does not capture the subtleties arising from the substantial degree of covalent character of the metal−sulfur bonds that has been shown to be crucial in the rationalization of the electronic structure in another apparently simple copper sulfide such as covellite[48] or in the mobility of copper in layered ternary sulfides derived from chalcopyrite.[49,50]

As mentioned above, the effects of the strong covalent character found for metal−sulfur bonds in chalcopyrite lead to the unexpected finding of a small, but non-negligible, spin density on the copper atoms for magnetic states of higher energy. As can be deduced from the values for the spin density collected in Table 2 or from the spin density plots in Figure 5, the spin density on the CuS_4 units is strongly dependent on the spin arrangement of the surrounding Fe^{3+} ions. Examining the calculated density of states (DOS) for the AFM and FM states (Figure 3), it can be seen that the Cu(3d) orbitals do not show a significant participation in the conduction band, either in the AFM or in the FM states. Furthermore, on analysis of the absolute values of the total and spin electronic densities for Fe, Cu, and S atoms in chalcopyrite obtained through the Mulliken population analysis, it becomes evident that the differences in the spin density on Cu between the AFM and FM states is not large (for more details, see the Supporting Information). All of these findings suggest that partial oxidation (participation of the Cu(3d) orbitals in the empty conduction band) is not responsible for the spin density found on the Cu atoms in the AFM′ and FM states.

DOI: 10.1021/acs.inorgchem.5b00399
Inorg. Chem. 2015, 54, 4840−4849

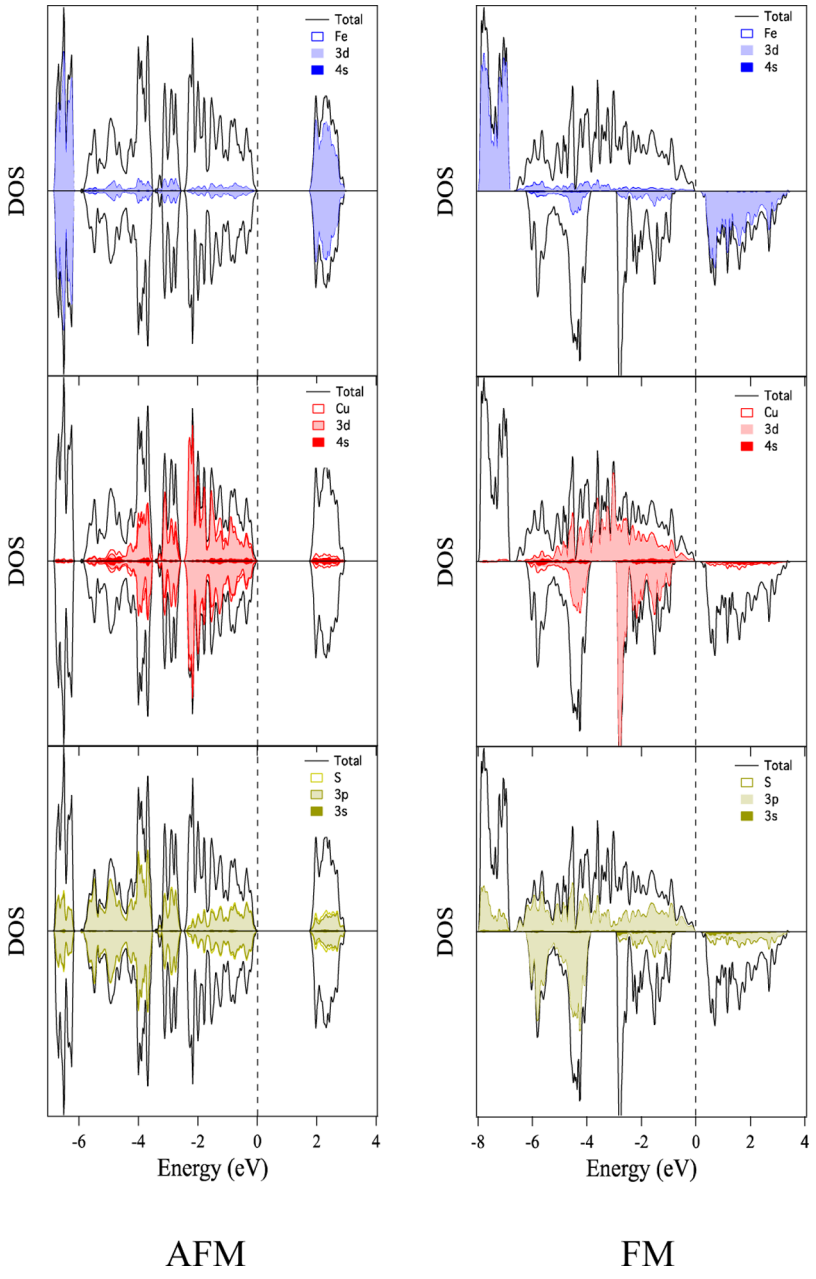

Figure 3. Total (DOS) and partial density of states (PDOS) for Fe, Cu, and S atoms calculated with the B3LYP functional for AFM and FM states.

On analysis of the density of states curves for Cu and S in the FM state (Figure 3) in more detail, the resulting small spin densities on the Cu atoms can be associated with an anomalous behavior in the valence band, for which the DOS curves corresponding to spin-up and spin-down electrons are not simply displaced one with respect to the other, as expected in the case of a partial oxidation, but differ also notably in shape. All of these observations indicate that the small spin densities in higher energy spin configurations, strongly dependent on the Fe^{3+} spin network, are a consequence to some degree of spin delocalization[51] over the CuS_4 units favored by the covalency in the M−S bonds in chalcopyrite.

An intriguing question is, however, why does this spin delocalization appear only for the AFM′ and FM states, and why is it substantially larger in the FM state if the spin densities on the iron atoms, and hence the covalent characters of metal−sulfur bonds, are similar in the three states? An answer to this question can be found by considering the geometry of the arrangement of iron atoms around a single CuS_4 tetrahedron (Figure 4).

As shown in Figure 4, there are eight iron atoms surrounding each CuS_4 tetrahedron in the chalcopyrite structure. The geometric arrangement of these eight atoms is that of a distorted gyrobifastigium, the 26th Johnson solid (J26), which can be constructed by joining two face-regular triangular prisms along corresponding square faces, giving a quarter-turn to one prism. The distances between the central copper atom and the eight iron atoms surrounding it are practically the same, with the distance to the four iron atoms lying on the same plane perpendicular to *c* of the copper atom (3.74 Å) being slightly longer than the distance to the other four Fe atoms located above and below this plane (3.71 Å).

In the lowest energy AFM state, the spin direction of Fe atoms alternates in successive planes perpendicular to the

DOI: 10.1021/acs.inorgchem.5b00399
Inorg. Chem. 2015, 54, 4840−4849

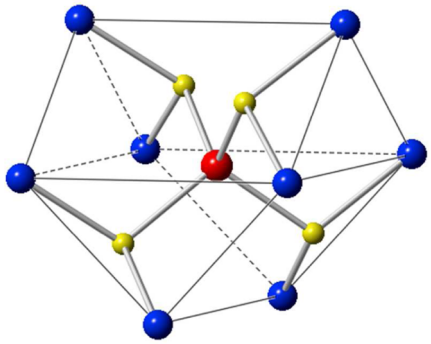

Figure 4. Geometric arrangement of iron Fe atoms (blue balls) around a single CuS_4 tetrahedron. The red ball corresponds to the Cu atom, and the small yellow balls correspond to the S atoms.

crystallographic *c* axis (Figure 2). For this reason we will find that the four atoms on the same plane as the central copper atom will have their spins aligned in a given direction, while the other four in the neighboring layers, two above and two below, will have the opposite direction. Since the distances of all eight Fe atoms to the copper atom are practically the same and, as seen in Figure 4, the eight Fe ions are each linked via a single sulfur atom to copper, it is evident that in this magnetic state, for symmetry reasons, the spin density on the iron atoms cannot induce a nonvanishing spin density on copper via a spin delocalization mechanism.

However, as the temperature increases, magnetic excitations take place on the subnet of Fe ions, forcing an increase of the population in magnetic configurations of the iron spins where the spin polarization on a CuS_4 tetrahedron is not longer canceled by symmetry. For the FM state, corresponding to the state of maximal magnetic excitation, we will find all eight iron atoms around a CuS_4 tetrahedron with their spins aligned in the same direction and the spin delocalization mechanism through the substantially covalent metal−sulfur bonds leading to a nonvanishing spin density on the atoms of the CuS_4 tetrahedra. Note in Figure 5 that the practically spherical distribution of the

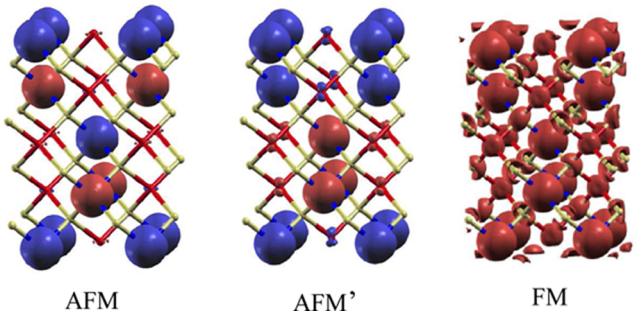

Figure 5. Spin density map for the AFM, AFM′, and FM spin distributions of $CuFeS_2$. The isodensity surface represented corresponds to a value of 0.010 e $bohr^{-3}$ for the three spin distributions (red regions indicate positive spin populations, and negative values are shown in blue).

eight iron spin densities of the same sign around the copper atom leads to a practically spherical spin density of the same sign on the copper atoms.

For the AFM′ state we find an intermediate situation between the AFM state, where spin polarization is impossible by symmetry, and the spherical spin density on copper found for the FM state, where all eight Fe^{3+} spins around each CuS_4 tetrahedron point in the same direction. In the AFM′ state, the spins of the four Fe atoms lying on the same layer as copper and the two spins lying in the layer above (or below) point in the same direction, while those on the layer below (or above) point in the opposite direction. The net result of spin delocalization through the M−S bonds in this case is a spin density on the copper atoms with the same sign as that of the four Fe atoms lying on the same plane. Since the spins of the Fe atoms above and below the plane containing the copper atom point in opposite directions, their contributions to spin delocalization on the copper atom cancel and the magnitude of the spin density on copper in this state is smaller than that in the FM state. As is evident from Figure 5, this spin density is now axially symmetric along the crystallographic *c* direction, in contrast with the almost spherical spin density found for the FM state.

This strange behavior suggests a strong dependence of the spin density on copper atoms with temperature or, in other words, a temperature-dependent magnetic moment on the copper atoms, associated with the ordering of the magnetic network of Fe ions, resulting in a complex magnetic behavior for copper in $CuFeS_2$ as a function of the temperature.

4.2. Exchange Coupling Constants. In order to give a stronger background to the conclusions on the magnetic behavior of $CuFeS_2$ obtained from electronic structure calculations, we decided to estimate a set of exchange coupling constants for the network of Fe^{3+} ($S = 5/2$) ions and use them afterward to simulate the susceptibility curve to compare it with our experimental data, where we expect to obtain a good fit considering only interactions between spins on the iron atoms: that is, using the approximation that copper atoms remain in a diamagnetic state as the temperature is increased.

Although several theoretical studies[20,42−45,52] on the electronic structure of $CuFeS_2$ have been previously reported, to the best of our knowledge, there has not been any attempt to explain the magnetic properties of this material by means of the determination of a set of magnetic coupling constants, J_i. To calculate the exchange coupling constants, we consider a Heisenberg−Dirac−van Vleck spin Hamiltonian that takes into account only pairwise interactions between spins:

$$\hat{H} = \sum_{i>j} J_{ij}\hat{S}_i\hat{S}_j \qquad (1)$$

where $\hat{S}_i$ and $\hat{S}_j$ are the spin operators of the different paramagnetic centers in the model and J_{ij} the exchange coupling constants describing the nature and strength of the interaction between them. On comparison with molecular systems,[53] in the case of extended solids, the Hamiltonian is in most cases considerably more complex due to the simultaneous presence of several exchange pathways with different *J* values.

The coupling constants were calculated according to the spin projection procedure. For a detailed discussion of the calculation of exchange coupling constants using first-principles methods and the approximations employed in projected and nonprojected cases, the interested reader is referred to the extensive literature on this topic.[52−61]

In order to evaluate in a correct way a complete set of coupling constants for $CuFeS_2$, it is necessary to consider at least a 2 × 1 × 1 supercell, as shown in Figure 6. From this figure it is also evident that it is not possible to calculate the J_b magnetic coupling constant using just the conventional cell,

DOI: 10.1021/acs.inorgchem.5b00399
Inorg. Chem. 2015, 54, 4840−4849

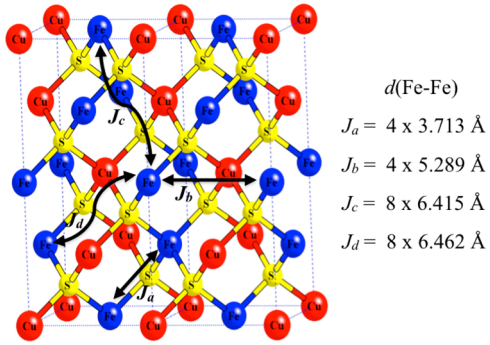

Figure 6. Schematic representation and Fe−Fe distances of the four exchange interactions in a 2 × 1 × 1 supercell.

because it would correspond to an interaction between two atoms equivalent by translational symmetry.

Despite the fact that hybrid functional methods provide a more reliable description of the electronic properties than DFT +U methods, the supercell calculations are difficult to carry out using the CRYSTAL program due to large computational requirements. For this reason the coupling constants will be evaluated only at the PBE+U level. Let us recall however that, as shown in Electronic and Magnetic Properties, for this particular case the results for the energy spacing between the magnetic configurations that can be built for a single conventional cell are very similar in the hybrid-DFT and DFT+U approaches (see Table 1), and for this reason we can assume that the coupling constants evaluated using the more affordable PBE+U calculations will be a good approximation to those that one would obtain using the B3LYP hybrid functional.

Energy differences between different spin configurations of the paramagnetic centers in the repeat unit of a given periodic model can be obtained in a simple way by associating pairwise interactions between neighbors to the coupling constants. The resulting equations and J_{ij} values (see the Supporting Information for more details about these calculations) for the four coupling constants in $CuFeS_2$ using energies per formula unit of the eight spin configurations shown in Figure 7 are

$$J_a = \frac{E_{A1} - E_{A2}}{25} = -82.2\ \text{K}$$

$$J_b = \frac{E_{A3} - E_{A4}}{25} = -13.7\ \text{K}$$

$$J_c = \frac{E_{A5} - E_{A4}}{25} = -5.3\ \text{K}$$

$$J_d = \frac{E_{A6} - E_{A7}}{25} = -5.2\ \text{K} \quad (2)$$

All four calculated exchange coupling constants are negative, or, in other words, correspond to antiferromagnetic interactions between two neighboring spins. As expected from simple structural arguments, the larger value corresponds to J_a, the coupling constant associated with the exchange path with a shorter Fe−Fe distance (3.713 Å) and a single bridging S atom linking the two paramagnetic Fe^{3+} ions. It is important to remark that the AFM antiferromagnetic ground state obtained with supercell calculations is in agreement with calculations described in Electronic and Magnetic Properties for the conventional cell as well as with the available experimental data.[4,8,10]

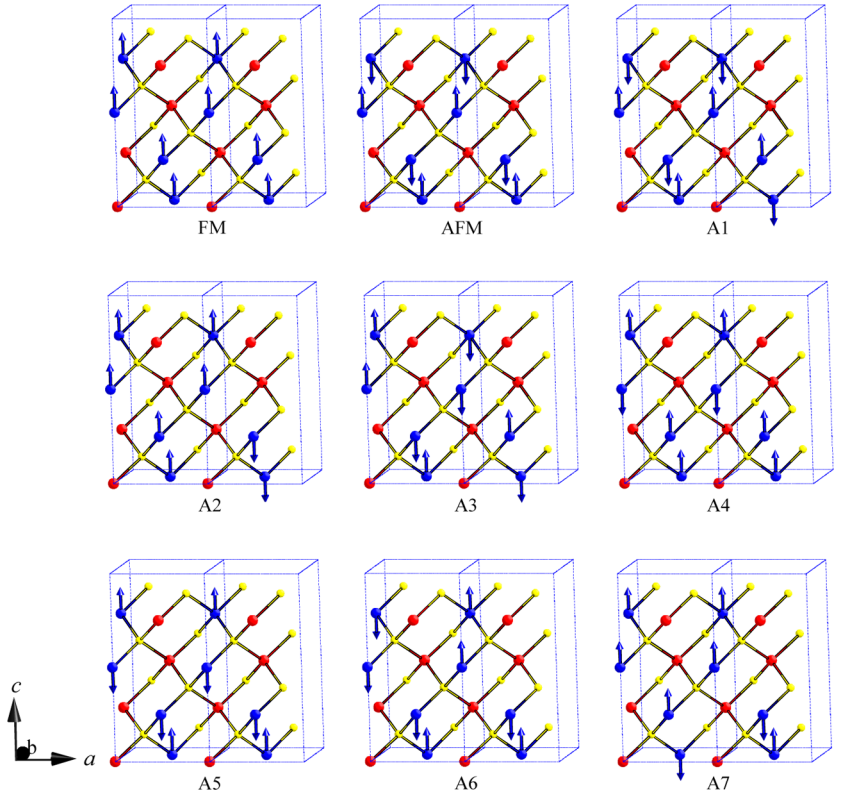

Figure 7. Schematic representation of the eight spin configurations considered for the evaluation of the magnetic properties in the 2 × 1 × 1 supercell. The most stable spin configuration (AFM) and the A5 magnetic configuration corresponding to AFM′ in Figure 2 have also been included.

DOI: 10.1021/acs.inorgchem.5b00399
Inorg. Chem. 2015, 54, 4840−4849

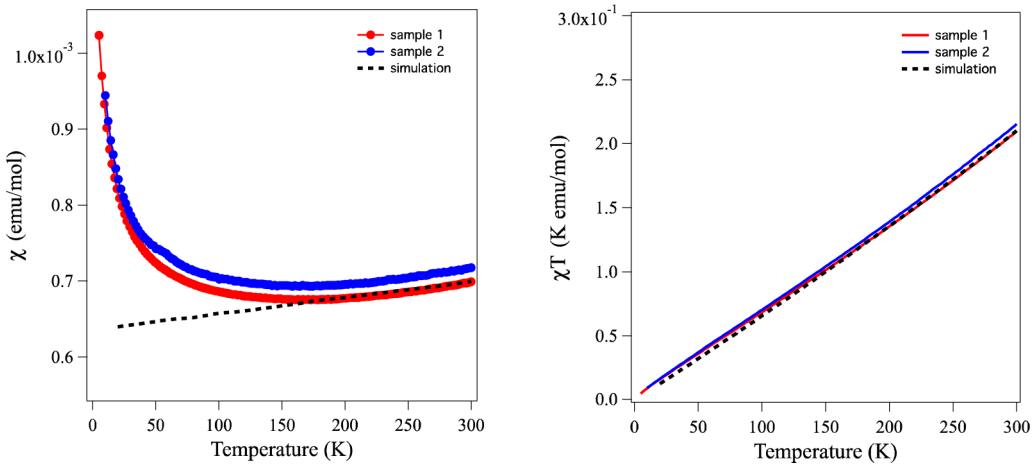

Figure 8. (left) Molar magnetic susceptibility data and (right) χT data for $CuFeS_2$ at 100 Oe and fit of the data corresponding to a model with the following coupling constants for Fe: $J_a = -171$ K, $J_b = -28.5$ K, $J_c = -10.4$ K, and $J_d = -10.2$ K.

4.3. Magnetic Susceptibility Curves. The measured molar magnetic susceptibility of $CuFeS_2$ as a function of the temperature using a field of 100 Oe is presented in Figure 8. The susceptibility (7.8×10^{-4} cm^3 mol^{-1} at 300 K) slightly decreases upon decreasing the temperature, reaching a minimum at ca. 175 K, with a value of 7.5×10^{-4} cm^3 mol^{-1}. This is indicative of an antiferromagnetic behavior with a high Néel temperature. The antiferromagnetic behavior is strong at room temperature, as reflected by the low value of the effective magnetic moment $\mu_{eff} = 2.83\ \chi T^{1/2} = 1.3\ \mu_B$ at room temperature. Below ~170 K, an increase in the magnetic molar susceptibility is observed. The abrupt increase of magnetic susceptibility at lower temperatures is probably due to minor amounts of paramagnetic impurities.

The susceptibility curve obtained for sample 2 presents a small cusplike anomaly at a temperature of 50 K, suggesting the onset of an additional antiferromagnetic ordering. As mentioned in the Introduction, in some previously reported work[9,10,13] this unusual behavior has been attributed to the magnetic ordering of the copper ions below 50 K. However, in our case the cusplike anomaly is not observed for sample 1, and we suggest that this behavior may probably be associated with the presence of a small amount of paramagnetic impurities rather than with an onset of additional antiferromagnetic ordering. This interpretation is also consistent with the fact that this anomaly is not observed if the measurements are carried out in a 5000 Oe magnetic field (see Figure S2 in the Supporting Information for more details).

To calculate the magnetic susceptibility for the Heisenberg model with the exchange coupling constants obtained from our first-principles calculations, we have performed classical Monte Carlo simulations including periodic boundary conditions (see Figure 8). The exchange coupling constants deduced from DFT calculations seem to underestimate the antiferromagnetic interactions in this case. This is confirmed by simulations performed on using the set of J values calculated with the PBE +U functional as a starting point and then fitting them to obtain a good agreement, above 170 K, with the experimental data (see Figure 8) while keeping the same ratio between the four J values as obtained in the DFT calculations. Such a procedure yields the following final values for the coupling constants: $J_a = -171$ K, $J_b = -28.5$ K, $J_c = -10.4$ K, and $J_d = -10.2$ K, which are about 2.1 times larger than those obtained from the DFT calculations.

Our simulations show that in the range 170−300 K it is not necessary to include the contribution of copper atoms in the model to reproduce adequately the magnetic susceptibility of $CuFeS_2$, which we take as indicative of the diamagnetic behavior for copper atoms as discussed above. To further sustain this hypothesis, we also carried out Monte Carlo calculations including the effect of paramagnetic Cu^{2+} ($S = 1/2$) ions in the range 170−300 K. In this case we find that it is not possible to obtain a good fit of the experimental data in that range of temperature, as in the case of considering copper to be in a diamagnetic state.

We wish to point out that the susceptibility at high temperatures is particularly well reproduced but, as expected, at low temperatures we are not able to explain the behavior of the magnetic susceptibility of $CuFeS_2$, mainly due to the well-known limitations of classical Monte Carlo simulations to describe correctly the magnetic behavior under conditions where quantum effects cannot be neglected and the possible effect of paramagnetic impurities, which have not been taken into consideration in our simulations.

5. CONCLUSIONS

The present study shows that the combination of electronic structure methods based on density functional theory and classical Monte Carlo simulations yields a plausible explanation of the magnetic properties of $CuFeS_2$ in the temperature range ~170−300 K, suggesting a diamagnetic behavior for copper atoms in this temperature range. Despite the fact that in our electronic structure calculations we observed small spin densities on the copper atoms in high-energy spin configurations, these are, however, not associated with a partial oxidation leading to empty 3d orbitals in the conduction band, as suggested in earlier works. The appearance of a small magnetic moment on the Cu^+ ions can, however, be understood by the fact that, as the temperature increases, magnetic excitations take place on the magnetic subnet of Fe spins, increasing the degree of spin delocalization on neighboring CuS_4 tetrahedra that gradually acquire a net spin moment. Apparently, as observed in the results obtained by Monte Carlo simulations, at the macroscopic level this small contribution would not have a significant effect on the magnetic

DOI: 10.1021/acs.inorgchem.5b00399
Inorg. Chem. 2015, 54, 4840−4849

susceptibility in the studied temperature range and it is only necessary to consider the iron spin network to obtain a good fit of the magnetic susceptibility curve. Although at lower temperatures our classical model is not appropriate to explain the magnetic behavior of $CuFeS_2$, our experimental results seem to indicate that the anomalous magnetic behavior at ~50 K reported in other works[9,10,13] may be more probably due to the presence of magnetic impurities than to a magnetic transition associated with the copper ions as suggested in the literature.

■ ASSOCIATED CONTENT

Supporting Information

Figures, text, and a table giving powder XRD patterns, molar magnetic susceptibility data at 100 and 5000 Oe, calculated total ($\rho = \alpha + \beta$) and spin ($\sigma = \alpha - \beta$) electronic densities, and detailed expressions for exchange coupling constants as a function of the energies of the different spin configurations shown in Figure 7. The Supporting Information is available free of charge on the ACS Publications website at DOI: 10.1021/acs.inorgchem.5b00399.

■ AUTHOR INFORMATION

Corresponding Authors

*P.A.: tel, (+34) 93 402 12 39; fax, (+34) 93 402 12 31; e-mail, p.alemany@ub.edu.

*I.de P.R.M.: tel, (+34) 93 403 92 89; fax, (+34) 93 402 12 31; e-mail, i.moreira@ub.edu.

Notes

The authors declare no competing financial interest.

■ ACKNOWLEDGMENTS

S.C. gratefully acknowledges the *Becas Chile* program (CONICYT PAI/INDUSTRIA 72090772) for a doctoral grant at the Universitat de Barcelona. The authors are indebted to Prof. Benjamín Martínez (ICMAB, CSIC) for his collaboration in the experimental measurements of the magnetic susceptibility of chalchopyrite. This work has been supported by the Spanish Ministerio de Economía y Competividad (MINECO) through research projects FIS2008-02238 and CTQ2012-30751 and by the *Generalitat de Catalunya* through projects 2014SGR301, 2014SGR97, and XRQTC.

■ REFERENCES

(1) Hulliger, F. *Struct. Bonding (Berlin)* **1968**, 83−229.

(2) Pearce, C. I.; Pattrick, R. A. D.; Vaughan, D. J.; Henderson, C. M. B.; Van der Laan, G. *Geochim. Cosmochim. Acta* **2006**, *70*, 4635−4642.

(3) Hall, S. R.; Stewart, J. M. *Acta Crystallogr., Sect. B: Struct. Sci.* **173**, *29*, 579−585.

(4) Donnay, G.; Corliss, L. M.; Donnay, J. D. H.; Elliott, N.; Hastings, J. M. *Phys. Rev.* **1958**, *112*, 1917−1923.

(5) Raj, D.; Chandra, K.; Puri, S. P. *J. Phys. Soc. Jpn.* **1968**, *24*, 39−41.

(6) Boekema, C.; Krupski, A. M.; Varasteh, M.; Parvin, K.; Van Til, F.; Van Der Woude, F.; Sawatzky, G. A. *J. Magn. Magn. Mater.* **2004**, *272*, 559−561.

(7) Sato, K.; Harada, Y.; Taguchi, M.; Shin, S.; Fujimori, A. *Phys. Status Solidi A* **2009**, *206*, 1096−1100.

(8) Engin, T. E.; Powell, A. V.; Hull, S. *J. Solid State Chem.* **2011**, *184*, 2272−2277.

(9) Woolley, J. C.; Lamarche, A. M.; Lamarche, G.; Quintero, M.; Swainson, I. P.; Holden, T. M. *J. Magn. Magn. Mater.* **1996**, *162*, 347−354.

(10) Knight, K. S.; Marshall, W. G.; Zochowski, S. W. *Can. Mineral.* **2011**, *49*, 1015−1034.

(11) Lovesey, S. W.; Knight, K. S.; Detlefs, C.; Huang, S. W.; Scagnoli, V.; Staub, U. *J. Phys.-Condens. Matter* **2012**, *24*, 216001.

(12) Teranishi, T. *J. Phys. Soc. Jpn.* **1961**, *16*, 1881−1887.

(13) Khabibullin, I. K.; Garif'yanov, N. N.; Matukhin, V. L. *Russ. Phys. J.* **2008**, *51*, 767−769.

(14) Rais, A.; Gismelseed, A. M.; Al-Rawas, A. D. *Mater. Lett.* **2000**, *46*, 349−353.

(15) Nikiforov, K. G. *Prog. Cryst. Growth Charact. Mater.* **1999**, *39*, 1−104.

(16) Fujisawa, M.; Suga, S.; Mizokawa, T.; Fujimori, A.; Sato, K. *Phys. Rev. B* **1994**, *49*, 7155.

(17) Llanos, J.; Buljan, A.; Mujica, C. *Mater. Res. Bull.* **1995**, *30*, 43−48.

(18) Mikhlin, Y.; Tomashevich, Y.; Tauson, V.; Vyalikh, D.; Molodtsov, S.; Szargan, R. *J. Electron Spectrosc. Relat. Phenom.* **2005**, *142*, 83−88.

(19) Todd, E. C.; Sherman, D. M.; Purton, J. A. *Geochim. Cosmochim. Acta* **2003**, *67*, 2137−2146.

(20) Goh, S. W.; Buckley, A. N.; Lamb, R. N.; Rosenberg, R. A.; Moran, D. *Geochim. Cosmochim. Acta* **2006**, *70*, 2210−2228.

(21) Haldane, F. D. M.; Anderson, P. W. *Phys. Rev. B* **1976**, *13*, 2553−2559.

(22) Bain, G. A.; Berry, J. F. *J. Chem. Educ.* **2008**, *85*, 532−536.

(23) See http://www.crystal.unito.it for details on the CRYSTAL code, Gaussian basis sets, computational schemes, etc.

(24) Dovesi, R.; Orlando, R.; Civalleri, B.; Roetti, C.; Saunders, V. R.; Zicovich-Wilson, C. M. *Z. Kristallogr.* **2005**, *220*, 571−573.

(25) Dovesi, R.; Saunders, V. R.; Roetti, R.; Orlando, R.; Zicovich-Wilson, C. M.; Pascale, F.; Civalleri, B.; Doll, K.; Harrison, N. M.; Bush, I. J.; Llunell, M. *CRYSTAL09 User's Manual*; University of Torino, Torino, Italy, 2009.

(26) Becke, A. D. *J. Chem. Phys.* **1993**, *98*, 5648−5652.

(27) Monkhorst, H. J.; Pack, J. D. *Phys. Rev. B* **1976**, *13*, 5188−5192.

(28) See http://departments.icmab.es/leem/siesta/ for details on the SIESTA code.

(29) For a review on applications of the SIESTA approach in materials science, see: Sánchez-Portal, D.; Ordejón, P.; Canadell, E. *Struct. Bonding (Berlin)* **2004**, *113*, 103−170.

(30) Soler, J. M.; Artacho, E.; Gale, J. D.; Garcia, A.; Junquera, J.; Ordejon, P.; Sanchez-Portal, D. *J. Phys.-Condens. Matter* **2002**, *14*, 2745−2779.

(31) Perdew, J. P.; Burke, K.; Ernzerhof, M. *Phys. Rev. Lett.* **1996**, *77*, 3865−3868.

(32) Hubbard, J. *Proc. R. Soc. London, Ser. A* **1963**, *A276*, 238−257.

(33) Dudarev, S. L.; Botton, G. A.; Savrasov, S. Y.; Humphreys, C. J.; Sutton, A. P. *Phys. Rev. B* **1998**, *57*, 1505−1509.

(34) Mosey, N. J.; Liao, P.; Carter, E. A. *J. Chem. Phys.* **2008**, *129*, 014103.

(35) Troullier, N.; Martins, J. L. *Phys. Rev. B* **1991**, *43*, 1993−2006.

(36) Kleinman, L.; Bylander, D. M. *Phys. Rev. Lett.* **1982**, *48*, 1425−1428.

(37) Artacho, E.; Sanchez-Portal, D.; Ordejon, P.; Garcia, A.; Soler, J. M. *Phys. Status Solidi B* **1999**, *215*, 809−817.

(38) Bauer, B.; Carr, L. D.; Evertz, H. G.; Feiguin, A.; Freire, J.; Fuchs, S.; Gamper, L.; Gukelberger, J.; Gull, E.; Guertler, S. *J. Stat. Mech. Theor. Exp.* **2011**, *2011*, P05001.

(39) Cano, J.; Journaux, Y. In *Magnetism: Molecules to Materials V*; Miller, J. S., Drillon, M., Eds.; Wiley-VCH: Weinheim, Germany, 2005; pp 189−222.

(40) Ruiz, E.; Llunell, M.; Cano, J.; Rabu, P.; Drillon, M.; Massobrio, C. *J. Phys. Chem. B* **2006**, *110*, 115−118.

(41) Pearce, C. I.; Pattrick, R. A. D.; Vaughan, D. J. *Rev. Mineral. Geochem.* **2006**, *61*, 127−180.

(42) Edelbro, R.; Sandström, Å.; Paul, J. *Appl. Surf. Sci.* **2003**, *206*, 300−313.

(43) de Oliveira, C.; Duarte, H. A. *Appl. Surf. Sci.* **2010**, *257*, 1319−1324.

DOI: 10.1021/acs.inorgchem.5b00399
Inorg. Chem. 2015, 54, 4840−4849

(44) Łażewski, J.; Neumann, H.; Parlinski, K. *Phys. Rev. B* **2004**, *70*, 195206.
(45) Klekovkina, V. V.; Gainov, R. R.; Vagizov, F. G.; Dooglav, A. V.; Golovanevskiy, V. A.; Pen'kov, I. N. *Opt. Spektrosk.* **2014**, *116*, 961−964.
(46) Rivero, P.; Moreira, I. de P. R.; Illas, F. *Phys. Rev. B* **2010**, *81*, 205123.
(47) Catti, M. *Phys. Rev. B* **1995**, *51*, 7441−7450.
(48) Conejeros, S.; Moreira, I. de P. R.; Alemany, P.; Canadell, E. *Inorg. Chem.* **2014**, *53*, 12402−12406.
(49) Conejeros, S.; Sánchez, V.; Llanos, J.; Alemany, P.; Padilla-Campos, L. *Z. Kristallogr.* **2010**, *225*, 475−477.
(50) Conejeros, S.; Alemany, P.; Llunell, M.; Sánchez, V.; Llanos, J.; Padilla-Campos, L. *Inorg. Chem.* **2012**, *51*, 362−369.
(51) Cano, J.; Ruiz, E.; Alvarez, S.; Verdaguer, M. *Comments Inorg. Chem.* **1998**, *20*, 27−56.
(52) Hamajima, T.; Kambara, T.; Gondaira, K. I.; Oguchi, T. *Phys. Rev. B* **1981**, *24*, 3349−3353.
(53) Kahn, O. *Molecular Magnetism*; VCH: New York, 1993.
(54) Llunell, M.; Alemany, P.; Moreira, I. de P. R. *Inorg. Chem.* **2009**, *48*, 5938−5945.
(55) Ruiz, E.; Llunell, M.; Alemany, P. *J. Solid State Chem.* **2003**, *176*, 400−411.
(56) Ruiz, E.; Cano, J.; Alvarez, S.; Alemany, P. *J. Comput. Chem.* **1999**, *20*, 1391−1400.
(57) Ruiz, E.; Alvarez, S.; Rodríguez-Fortea, A.; Alemany, P.; Pouillon, Y.; Massobrio, C. In *Magnetism: Molecules to Materials Molecule-based Materials*; Miller, J. S., Drillon, M., Eds.; Wiley-VCH: Weinheim, Germany, 2001; pp 227−279.
(58) Ruiz, E.; Rodríguez-Fortea, A.; Cano, J.; Alvarez, S.; Alemany, P. *J. Comput. Chem.* **2003**, *24*, 982−989.
(59) Caballol, R.; Castell, O.; Illas, F.; Moreira, I. de P. R.; Malrieu, J. P. *J. Phys. Chem. A* **1997**, *101*, 7860−7866.
(60) Moreira, I. de P. R.; Illas, F. *Phys. Chem. Chem. Phys.* **2006**, *8*, 1645−1659.
(61) Moreira, I. de P. R.; Calzado, C. J.; Malrieu, J. P.; Illas, F. *New J. Phys.* **2007**, *9*, 369−394.

DOI: 10.1021/acs.inorgchem.5b00399
Inorg. Chem. 2015, 54, 4840−4849